Research Square

Preprints are preliminary reports that have not undergone peer review.
They should not be considered conclusive, used to inform clinical practice,
or referenced by the media as validated information.

Umbilical Cord Mesenchymal Stem Cells Alleviate Osteoblast Differentiation Disorder Induced by Oxidative Stress by Inhibiting Ferroptosis Through the miR-218-5p/CBX3 Axis

Lintong Li
Third People's Hospital of Yunnan Province
Yunda Huang
Third People's Hospital of Yunnan Province
Yuan Ma
Third People's Hospital of Yunnan Province
Jiaxin Liu
Kunming University of Science and Technology
Yu Chang
cyjx2115250163.com
Third People's Hospital of Yunnan Province

Research Article

Keywords: Osteoporosis, Umbilical cord mesenchymal stem cells, Ferroptosis, miR-218-5p, CBX3, Osteogenic differentiation, Oxidative stress

Posted Date: September 10th, 2026

DOI: https://doi.org/10.21203/rs.3.rs-10663759/v1

License: This work is licensed under a Creative Commons Attribution 4.0 International License.
Read Full License

Additional Declarations: No competing interests reported.

Abstract

Objective

The pathogenesis of osteoporosis is closely linked to osteoblast impairment caused by oxidative stress. While umbilical cord mesenchymal stem cells (UC-MSCs) are widely recognized as a promising regenerative therapy, the specific pathways underlying their protective effects on oxidatively stressed osteoblasts are not fully understood. This study aimed to determine whether UC-MSCs exerted protective effects on osteoblasts by targeting ferroptosis and to characterize the mediating function of the miR-218-5p/CBX3 signaling axis in this regulatory mechanism.

Methods

We established an *in vitro* oxidative stress injury model by treating the mouse osteoblast cell line (MC3T3-E1) with H_2O_2. We co-cultured these cells with UC-MSCs. Cell viability and injury were evaluated using CCK-8 and LDH release assays. ROS, Fe^{2+}, MDA, and glutathione (GSH) levels were assessed with probes and biochemical kits to evaluate ferroptosis characteristics. Expression of ferroptosis defense proteins and osteogenic markers was analyzed using RT-qPCR and Western blot analysis. To validate the regulatory relationship between miR-218-5p and CBX3, dual-luciferase reporter assays were employed. Functional rescue experiments were carried out using a specific ferroptosis inducer (RSL3), miRNA inhibitors, overexpression constructs, and siRNA-mediated gene silencing.

Results

UC-MSCs protected MC3T3-E1 cells from H_2O_2 injury by improving viability, reducing LDH release, and inhibiting ferroptosis (ROS, iron overload, lipid peroxidation). They upregulated glutathione peroxidase 4 (GPX4), SLC7A11, and FTH, restoring ALP activity and osteogenic marker expression. Importantly, the introduction of RSL3 entirely abrogated these UC-MSC-mediated osteoprotective effects, confirming the causal involvement of ferroptosis. Mechanism studies showed that H_2O_2 downregulated the expression of miR-218-5p, which directly targets the 3'UTR of CBX3 and inhibited its protein expression; UC-MSCs could significantly upregulate and restore miR-218-5p levels. Mechanism studies have shown that miR-218-5p effectively replicates the anti-ferroptosis and bone protection effects of UC-MSCs. On the contrary, the use of specific inhibitors to suppress miR-218-5p significantly weakened the protective benefits of UC-MSCs against ferroptosis and osteogenic dysfunction, and the overexpression of CBX3 also reversed the protective effect mediated by UC-MSCs.

Conclusion

UC-MSCs inhibit oxidative stress-induced osteoblast ferroptosis and promote osteogenesis via the miR-218-5p/CBX3 axis, providing new insights into MSC therapy for osteoporosis.

1 Introduction

Osteoporosis is a prevalent global public health issue characterized by progressive bone mineral loss and deterioration of bone microarchitecture, conditions that markedly increase susceptibility to fragility fractures(Hernlund et al. 2013; Salari *et al.* 2021). Bone health is maintained by a tightly regulated balance between osteoblast-mediated bone formation and osteoclast-mediated bone resorption(Manolagas 2000). The aging process promotes ROS accumulation in the bone marrow, creating a highly oxidative microenvironment that drives osteoblast apoptosis, senescence, and impaired differentiation(Ye *et al.* 2023; Shen *et al.* 2022). In recent years, therapeutic strategies utilizing umbilical cord mesenchymal stem cells (UC-MSCs) have emerged as a promising approach in bone tissue engineering and the management of metabolic bone diseases, owing to their potent paracrine immunomodulatory, free radical-scavenging, and niche-remodeling activities(Li *et al.* 2024; Liu et al. 2018). However, the specific molecular signaling networks downstream of UC-MSCs that confer osteoprotection against oxidative stress-related damage remain incompletely understood.

Ferroptosis is a newly identified form of regulated cell death, defined by the toxic accumulation of iron-driven lipid peroxidation products that culminate in cell demise. The onset of ferroptosis is commonly associated with marked depletion of glutathione (GSH) and the loss of activity of essential antioxidant defense components such as glutathione peroxidase 4 (GPX4)(Ru *et al.* 2024; Dixon *et al.* 2024). Increasing studies have shown that iron homeostasis imbalance plays a crucial pathological role in various types of osteoporosis(Ruan *et al.* 2024). When osteoblasts are subjected to severe oxidative stress, ferroptosis is easily induced, directly leading to the loss of bone formation ability(Wang *et al.* 2024). Therefore, targeting the inhibition of osteoblast ferroptosis is considered a highly promising anti-osteoporosis targeted strategy. In this context, exploring whether UC-MSCs can exert their bone protection function by intervening in the ferroptosis metabolic pathway holds significant scientific significance.

Mesenchymal stem cells (MSCs), especially umbilical cord-derived UC-MSCs, possess strong paracrine functions and immunomodulatory capabilities, and have shown promising application prospects in tissue repair and bone regeneration(Rahyussalim et al. 2023). Previous studies have shown that UC-MSCs alleviate oxidative stress damage by secreting exosomes and cytokines, but the specific molecular mechanism of their regulation of osteoblast ferroptosis remains to be systematically elucidated. MicroRNAs (miRNAs) are important epigenetic regulatory factors that play a crucial role in maintaining bone metabolic homeostasis(Iantomasi *et al.* 2023; Philippe et al. 2023). miR-218-5p is abnormally expressed in various bone disease models and has been reported to promote osteoblast differentiation and alleviate postmenopausal osteoporosis by targeting SOCS3(Zhou *et al.* 2023); while CBX3 (Chromobox 3), as the core component of the polycomb repressive complex (PRC1), participates

in chromatin remodeling and gene transcription regulation and may play an important role in cellular stress responses and differentiation(Wu *et al.* 2026).

In this study, we established an *in vitro* model of oxidative stress in mouse osteoblasts (MC3T3-E1) using H_2O_2. Based on previous observations, we hypothesized that under severe oxidative stress stimulation, the pathogenic factor CBX3 in osteoblasts would be abnormally highly expressed, thereby serving as a key hub to induce ferroptosis and inhibit osteogenic differentiation; while UC-MSCs could precisely target and inhibit the transcription and translation of CBX3 by upregulating miR-218-5p, thereby establishing an anti-ferroptosis barrier and salvaging osteogenic function. The primary objective of this study was to uncover the molecular mechanisms underlying UC-MSC treatment for osteoporosis. These findings aim to inform the design of new bone-preserving approaches based on miRNA-mediated epigenetic regulation.

2 Materials and Methods

2.1 Cell Culture and Processing

MC3T3-E1 was obtained from the Chinese Academy of Sciences Cell Bank. UC-MSCs (CP-CL11, China Punosai) were purchased from Wuhan Punosai Life Science and Technology Co. According to the manufacturer's instructions, these cells were isolated from human umbilical cord tissue and phenotypically analyzed in accordance with the multi-potential mesenchymal stem cell definition standards proposed by the International Society for Cellular Therapy (ISCT). Through flow cytometry verification, these cells were positive for the classic MSC surface markers CD73, CD90, and CD105 (positive rate > 95%), and negative for hematopoietic markers CD34 and CD45 (positive rate < 2%). Additionally, the cells exhibited the ability to differentiate into three lineages: osteogenic differentiation was confirmed by alizarin red S staining of mineralized matrix, adipogenic differentiation was confirmed by oil red O staining of lipid droplets, and chondrogenic differentiation was evaluated by alcian blue staining of matrix rich in glycosaminoglycans. All experiments were conducted using the 3rd to 6th generations (P3–P6) of UC-MSCs. MC3T3-E1 cells were maintained in α-MEM with 10% FBS and 1% penicillin/streptomycin at 37°C, 5% CO_2. Three experimental groups were established: a control group (Ctrl), an H_2O_2-induced treated group (200 μmol/L H_2O_2 treatment for 24 h), and a co-culture group in which UC-MSCs and MC3T3-E1 cells were separated using a Transwell system (UC-MSCs in the upper chamber, MC3T3-E1 in the lower well). In subsequent mechanistic assays, cells in each group were further treated with relevant inhibitors, plasmids, or oligonucleotides on this foundation.

2.2 Cell Viability and Membrane Damage Detection

The cytotoxicity of H_2O_2 and the protective effects of UC-MSCs were evaluated by measuring cell viability using the CCK-8 detection kit (Beijing Beyotime Biotechnology Co., Ltd., Cat. No. C0038). MC3T3-E1 cells were seeded into 96-well plates at a density of 5×10³ cells/well. After treatment for different durations (0, 12, 24, 36, and 48 hours), 10 μL of CCK-8 reagent was added to each well, followed by a 1.5-hour incubation period. Absorbance values at 450 nm were subsequently recorded. Concurrently, culture

supernatants were collected to measure LDH leakage using the LDH Assay Kit (Beijing Beyotime Biotechnology Co., Ltd., Cat. No. C0017), which served as an indicator of cell membrane damage and cytotoxicity.

2.3 Detection of Intracellular Reactive Oxygen Species (ROS)

The accumulation of intracellular ROS was quantified using a DCFH-DA fluorescent assay (Beyotime, Cat. No. S0033). Briefly, the treated cells underwent triple washing with PBS before a 30-min incubation with 10 μmol/L DCFH-DA (prepared in serum-free conditions) at 37°C, protected from light. Residual unbound probes were subsequently removed by rinsing with PBS three times. An Olympus IX73 microscope (Japan) was employed to capture the green fluorescent signals, which were then processed by ImageJ software (NIH, USA) to calculate the mean fluorescence intensity.

2.4 Determination of Biochemical Indicators of Ferroptosis (Fe^{2+}, MDA, GSH)

According to the instructions of the kit, a biochemical quantitative analysis was conducted on the core markers of ferroptosis in the cells. All the kits were purchased from Nanjing Jiancheng Bioengineering Institute. The ferroin (Fe^{2+}) assay kit (Nanjing Jiancheng, Cat. No. A039-2-1) was used to detect the concentration of free Fe^{2+} in the cells.

2.5 Oligonucleotide and Plasmid Transfection

The specific inhibitors, mimics, and their respective negative controls (NC) targeting miR-218-5p, as well as the small interfering RNA (si-CBX3) targeting CBX3 and its negative control (si-NC), were all synthesized by GenePharma (Suzhou, China). Shanghai GeneChem Co., Ltd. (China) provided the empty vector (oe-NC) alongside the expression plasmid encompassing the entire mouse *Cbx3* cDNA sequence (oe-CBX3). Upon reaching a confluence of approximately 60–70%, the MC3T3-E1 cultures underwent transient transfection. This procedure was facilitated by the Lipofectamine 3000 kit (Invitrogen, Carlsbad, CA, USA), strictly adhering to the established protocol provided by the supplier. At 48 h post-transfection, the cellular samples were harvested for further assays or applied in the co-culture system. Additionally, in specific mechanism reversal experiments, 5 μM ferroptosis-specific inducer RSL3 (MedChemExpress, USA, Cat. No. HY-100218) was added for intervention treatment.

2.6 Osteogenic Differentiation Induction and Detection

Osteogenic differentiation of MC3T3-E1 cells was induced by culturing them in differentiation medium containing α-MEM supplemented with 10 mM β-glycerophosphate, 50 μg/mL ascorbic acid, and 100 nM dexamethasone. At 7 and 14 days post-induction, ALP activity was assessed with the commercial assay kit (Nanjing Jiancheng Biotechnology Institute, Cat. No. A059-2-2), following the provided protocol. The assay employed pNPP as the substrate, and absorbance values were recorded at 405 nm to calculate

ALP activity. The measured ALP levels were then normalized against total protein content, which was determined using the BCA method.

2.7 Real-time Fluorescence Quantitative PCR (RT-qPCR)

Cellular total RNA was extracted by employing the TRIzol reagent (Cat. No. 9109; Takara Bio, Japan). Following the evaluation of RNA yield and quality via a NanoDrop 2000 device (Thermo Fisher Scientific, USA), 1 μg of the extracted RNA was synthesized into complementary DNA (cDNA) using the HiScript III RT SuperMix kit (Cat. No. R323-01; Vazyme Biotech, Nanjing, China). Subsequent fluorescent quantitative PCR was executed using the ChamQ Universal SYBR Green Master Mix (Cat. No. Q711-02; Vazyme Biotech). The amplification processes were monitored on either a Bio-Rad CFX Connect or an Applied Biosystems QuantStudio 5 thermocycler. To calculate the relative transcriptional abundance of the genes of interest (miR-218-5p, Alp, Ocn, and Runx2), the standard $2^{-\Delta\Delta Ct}$ algorithm was applied. For the mRNA expressions (Alp, OCN, Runx2, and CBX3), β-actin was used as the endogenous normalization control; for the expression of miR-218-5p, U6 small nuclear RNA (snRNA) was employed for normalization. The specific primer sequences used were as follows: β-actin (Forward: 5'-CACCATTGGCAATGAGCGGTTC-3', Reverse: 5'-AGGTCTTTGCGGATGTCCACGT-3'); ALP (Forward: 5'-GGGGTACAAGGCTAGATGGC-3', Reverse: 5'-GAGAGCGAAGGGTCAGTCAG-3'), OCN (Forward: 5'-GTCCAAGCAGGAGGGCAATA-3', Reverse: 5'-GATGCGTTTGTAGGCGGTCT-3'), Runx2 (Forward: 5'-AATGATGAGAACTACTCCGCCG-3', Reverse: 5'-GCCTGCCTGGGATTTCTTGGT-3'), CBX3 (Forward: 5'- TAGATCGACGTGTAGTGAATGGG-3', Reverse: 5'-TGTCTGTGGCACCAATTATTCTT-3'); U6 (Forward: 5'-CTCGCTTCGGCAGCACA-3', Reverse: 5'-AACGCTTCACGAATTTGCGT-3'); miR-218-5p (Forward: 5'-GCGCGTTGTGCTTGATCTAA-3', Reverse: 5'-AGTGCAGGGTCCGAGGTATT-3').

2.8 Western Blot Analysis

For protein expression profiling, cellular lysates were prepared in RIPA buffer (Beyotime, Shanghai, China) containing a cocktail of protease and phosphatase inhibitors. Following protein concentration determination via a BCA assay, standardized aliquots (20–30 μg) of protein were resolved on SDS-PAGE gels and subsequently transferred to PVDF membranes. To prevent non-specific binding, the blots were incubated in a 5% skim milk blocking solution for 60 min at ambient temperature. This was followed by an overnight incubation at 4°C with specific primary antibodies targeting GPX4, SLC7A11, FTH1, CBX3, ALP, OCN, RUNX2, and β-actin. The detailed information for the primary antibodies used is: anti-GPX4 (Abcam, ab125066, 1:1000), anti-SLC7A11 (CST, #12691, 1:1000), anti-FTH1 (Proteintech, 11827-1-AP, 1:1000), anti-CBX3 (Abcam, ab210903, 1:2000), anti-ALP (Santa Cruz, sc-271431, 1:500), anti-OCN (Abcam, ab13418, 1:1000), anti-RUNX2 (CST, #12556, 1:1000), and anti-β-actin (Sigma, A5441, 1:5000). After thorough washing steps the next day, the blots were exposed to HRP-linked secondary antibodies for another hour at room temperature. Finally, immunoreactive signals were detected using an ECL reagent, with densitometric quantification executed by ImageJ software.

2.9 Dual Luciferase Reporter Gene Assay

To elucidate the direct interaction between miR-218-5p and CBX3, a dual-luciferase reporter system was utilized. The wild-type 3'-untranslated region (3'UTR) of CBX3, harboring the putative miR-218-5p complementary site, alongside its mutated counterpart, was cloned into pmirGLO plasmids. MC3T3-E1 cells in the exponential growth phase were seeded into 24-well culture dishes. Subsequently, these cells underwent co-transfection with the constructed wild-type or mutant reporter vectors in combination with either miR-218-5p mimics or negative control oligos (miR-NC). Following a 48-h incubation period, the cellular lysates were collected. The luminescence levels generated by firefly and Renilla luciferases were ultimately evaluated employing a dual-luciferase reporter assay system (Promega, USA), which facilitated the calculation of the relative luminescent ratios.

2.10 Function Restoration Experiment

The miR-218-5p inhibitor (or mimic) and the CBX3 overexpression plasmid were transfected into MC3T3-E1 cells to verify their effects on the protection of UC-MSCs.

2.11 Statistical Analysis

GraphPad Prism software (version 8.0) was used as the main tool for all statistical calculations in this study. All experiments were conducted in three independent biological replicates, with each replicate containing at least three technical replicates. Quantitative results were expressed as the mean ± standard deviation. Statistical comparisons between two groups were performed using the unpaired Student's t-test, while comparisons among three or more groups were conducted using one-way analysis of variance (ANOVA), followed by Tukey's post hoc test. A *P* value less than 0.05 was considered statistically significant.

3 Results

3.1 UC-MSCs can rescue osteoblast damage and differentiation disorders induced by oxidative stress by inhibiting ferroptosis

This study aims to investigate whether UC-MSCs in bone cells can alleviate oxidative stress-mediated damage and clarify the underlying regulatory mechanism. An oxidative stress injury model was established by treating MC3T3-E1 cells with H_2O_2, and the role of RSL3 (a specific ferroptosis inducer) was verified in a partial co-culture system. The results showed that H_2O_2 significantly reduced cell viability within 48 hours, and co-culture with UC-MSCs effectively alleviated this cytotoxic effect (Fig. 1A). Similarly, H_2O_2 treatment led to a significant increase in LDH release, while UC-MSCs intervention could significantly inhibit this phenomenon (Fig. 1B, $P < 0.0001$). Since oxidative stress is the main driver of ferroptosis, we further evaluated the indicators related to ferroptosis. DCFH-DA staining showed that H_2O_2 induced a sharp accumulation of intracellular ROS in cells, while UC-MSCs significantly cleared excessive ROS (Fig. 1C, D). At the protein level, UC-MSCs significantly upregulated the expression of key ferroptosis defense markers, including GPX4, SLC7A11, and FTH, which were

downregulated in H_2O_2 treatment (Fig. 1E-H). Notably, after introducing RSL3, the protective effect of UC-MSCs on cell survival and inhibition of ferroptosis was significantly weakened, indicating that the anti-ferroptosis effect is crucial for UC-MSC-mediated cell protection. Additionally, we also evaluated the effect of UC-MSCs on osteogenic differentiation. RT-qPCR and Western blot analysis showed that H_2O_2 exposure severely inhibited the expression of osteogenic-related markers (including ALP, OCN, and Runx2) at the mRNA and protein levels (Fig. 1L-O). While UC-MSC treatment could effectively restore the expression of these markers. However, this osteogenic repair was mostly reversed after RSL3 treatment.

3.2 UC-MSCs mediate anti-ferroptosis effects via miR-218-5p and rescue osteogenic differentiation defects

To elucidate the molecular mechanisms underlying the protective effects of UC-MSCs, we focused on the regulatory role of miR-218-5p. First, RT-qPCR results showed that H_2O_2-induced oxidative stress significantly suppressed miR-218-5p expression, whereas co-culture with UC-MSCs markedly upregulated its levels (Fig. 2A-B). Subsequently, functional rescue experiments confirmed the central role of miR-218-5p in resisting ferroptosis. Results indicated that addition of a miR-218-5p inhibitor significantly weakened UC-MSCs' ability to clear ROS accumulation, Fe^{2+}, and MDA (Fig. 2C-F), while also exacerbating GSH depletion (Fig. 2G). At the protein level, the miR-218-5p inhibitor significantly downregulated the expression of ferroptosis defense proteins—GPX4, SLC7A11, and FTH—that were induced by UC-MSCs (Fig. 2H-K). These findings suggest that upregulation of miR-218-5p is a critical step in UC-MSC-mediated suppression of ferroptosis. Furthermore, we evaluated the impact of miR-218-5p on osteogenic differentiation at both transcriptional and translational levels. RT-qPCR revealed that, compared to the UC-MSC co-culture group, addition of the miR-218-5p inhibitor significantly reduced mRNA expression of osteogenic genes ALP, OCN, and Runx2 (Fig. 2L-N, $P < 0.0001$). Consistently, Western blot analysis demonstrated that inhibition of miR-218-5p significantly counteracted the restorative effect of UC-MSCs on the expression of these osteogenic proteins (Fig. 2O-R).

3.3 miR-218-5p directly targets and negatively regulates the expression of CBX3

To reveal the downstream molecular mechanism by which miR-218-5p protects osteoblasts, we predicted through bioinformatics databases that the 3'UTR region of CBX3 contains potential binding sites for miR-218-5p (Fig. 3A). To verify this prediction, we constructed a CBX3 3'UTR luciferase reporter vector containing the wild-type (WT) or mutant (Mut) binding sequences. The dual-luciferase reporter gene assay results showed that transfection with miR-218-5p mimics significantly reduced the luciferase activity of the CBX3-WT vector ($P = 0.0034$), while having no significant effect on the luciferase activity of the CBX3-Mut vector (Fig. 3B), confirming the direct binding of miR-218-5p to CBX3 mRNA. Subsequently, we evaluated the regulatory effect of miR-218-5p on CBX3 protein expression. Western blot results showed that H_2O_2 treatment led to a significant increase in the protein level of CBX3 in

MC3T3-E1 cells (Fig. 3C-D, P = 0.0002). After transfection with miR-218-5p mimic on top of H_2O_2 treatment, the expression level of CBX3 protein was significantly inhibited (*P* = 0.0004).

3.4 Targeted knockdown of endogenous CBX3 can simulate the anti-ferroptosis and bone protection effects of UC-MSCs

Given that miR-218-5p has been confirmed to have a negative regulatory effect on CBX3, we further used small interfering RNA (si-CBX3) to directly silence CBX3 in MC3T3-E1 cells, aiming to verify whether inhibiting this factor is sufficient to produce a bone protection effect similar to that of UC-MSCs. Western blot results confirmed the knockdown efficiency: H_2O_2 treatment significantly induced an increase in CBX3 expression (Fig. 4A-B, P = 0.0164), while after transfection with si-CBX3, its protein level was significantly downregulated under oxidative stress conditions (*P* = 0.0009). Subsequently, we evaluated the effects of silencing CBX3 on cell phenotype and the ferroptosis pathway. DCFH-DA fluorescence staining showed that knockdown of CBX3 significantly reduced the intracellular ROS accumulation induced by H_2O_2 (Fig. 4C-D, P < 0.0001). At the molecular level, Western blot results confirmed that inhibiting the expression of CBX3 significantly restored the levels of ferroptosis defense proteins GPX4, SLC7A11, and FTH (Fig. 4E-H), indicating that CBX3 is a potential key target mediating the occurrence of ferroptosis under oxidative stress. Finally, we detected changes in osteogenic differentiation markers. The results showed that silencing CBX3 significantly alleviated the inhibition of osteogenic function by H_2O_2. At the protein level, the expressions of Runx2, ALP, and OCN were significantly restored (Fig. 4I-L); at the same time, RT-qPCR results also confirmed the synchronous upregulation of these osteogenic-related genes at the mRNA level (Fig. 4M-O, P < 0.0001). These results suggest that by directly inhibiting the expression of CBX3 through genetic means, it is possible to simulate the anti-ferroptosis effect of UC-MSCs, thereby effectively rescuing the osteogenic differentiation disorder caused by oxidative stress.

3.5 Overexpression of CBX3 weakened the anti-ferroptosis and osteogenic rescue effects of UC-MSCs on osteoblasts

After confirming the protective effect of silencing CBX3, we further verified the necessity of the miR-218-5p/CBX3 axis in UC-MSC treatment through functional restoration experiments. We transfected the CBX3 overexpression plasmid (Oe-CBX3) into the co-culture system to observe whether it could reverse the bone protective effect of UC-MSCs. The results showed that UC-MSCs significantly reduced the ROS accumulation, Fe^{2+}, and MDA levels induced by H_2O_2, and restored the GSH reserves; however, the introduction of Oe-CBX3 significantly weakened these anti-ferroptosis effects (Fig. 5A-E). At the molecular level, Western blot results showed that overexpression of CBX3 significantly downregulated the expression of iron death defense proteins (GPX4, SLC7A11, and FTH) maintained by UC-MSCs (Fig. 5F-D). Meanwhile, the rescue effect of UC-MSCs on osteogenic differentiation function was significantly blocked by Oe-CBX3. RT-qPCR results showed that compared with the control plasmid

group, overexpression of CBX3 led to a significant decrease in the mRNA levels of key osteogenic genes ALP, OCN, and Runx2 (Fig. 5J-L, $P < 0.0001$). Similarly, Western blot results also confirmed the synchronous decline of these osteogenic markers at the protein expression level (Fig. 5M-P).

4 Discussion

Osteoporosis is characterized by a progressive deterioration of the bone marrow microenvironment. Notably, the persistent oxidative stress triggered by aging or the sharp decline in hormone levels following menopause is considered a core pathological driver that impairs the osteogenic function of osteoblasts(Subarajan et al. 2024; Fischer *et al.* 2022; Yao *et al.* 2025). In recent years, UC-MSCs have attracted much attention in the cell therapy of metabolic bone diseases due to their outstanding paracrine immune regulation and microenvironment remodeling capabilities(Hoang *et al.* 2022; Zhidu *et al.* 2024). However, the underlying epigenetic and metabolic coupling mechanism by which UC-MSCs enable osteoblasts to resist oxidative stress damage has not yet been fully unraveled. This study clarifies a previously uncharacterized molecular defense mechanism through which UC-MSCs exert their cytoprotective effects: UC-MSCs can precisely target and downregulate the expression of the pathogenic hub gene CBX3 by upregulating miR-218-5p in damaged osteoblasts, thereby attenuating osteoblast ferroptosis induced by H_2O_2 and substantially restoring their osteogenic differentiation potential. This discovery not only provides a new perspective for understanding the bone-protective effect of UC-MSCs, but also greatly enriches the ferroptosis metabolic theory of osteoporosis.

Defined as a regulated form of cell death, ferroptosis is characterized by iron-dependent lipid peroxidation and is implicated in the progression of multiple oxidative stress-associated pathologies, such as osteoporosis(Dixon *et al.* 2014; Battaglia *et al.* 2020; Xia *et al.* 2023). In this study, it was observed that H_2O_2 treatment significantly induced ferroptosis in MC3T3-E1 cells, characterized by excessive accumulation of ROS, increased intracellular Fe^{2+} levels, increased MDA content, depletion of GSH, and downregulation of GPX4, SLC7A11, and FTH at both mRNA and protein levels. Co-culture with UC-MSCs effectively reversed these ferroptosis-related phenotypes and restored osteogenic differentiation ability(Svajger et al. 2025; Shen *et al.* 2019). To further verify the mediating role of ferroptosis in oxidative stress-induced osteogenic dysfunction, we introduced the GPX4-specific inhibitor RSL3(Kim et al. 2023; Xiao *et al.* 2025). The results showed that RSL3 significantly weakened the protective effect of UC-MSCs on osteogenic differentiation, confirming that ferroptosis is the critical downstream mediator of H_2O_2-induced osteogenic cell dysfunction, which is consistent with recent reports on targeting ferroptosis to improve bone metabolic disorders.

When exploring the upstream regulatory mechanism of the anti-ferroptosis effect of UC-MSCs, we focused on the epigenetic regulation mediated by microRNAs. UC-MSCs can transfer miRNAs through paracrine pathways (including exosomes) and reconfigure the gene expression network of target cells(Zhang *et al.* 2022; Xu et al. 2021; Saadh *et al.* 2025). This study found that H_2O_2 stimulation significantly downregulated the expression of miR-218-5p in MC3T3-E1 cells, while co-culture with UC-MSCs could effectively rescue this downregulation. Applying miR-218-5p-specific inhibitors can weaken

the anti-ferroptosis and osteogenic protective effects of UC-MSCs, leading to a secondary decrease in the expression of osteogenic markers (ALP, OCN, Runx2) and ferroptosis defense genes (GPX4, SLC7A11, FTH) at the transcriptional level, indicating that miR-218-5p is an important downstream effector molecule for the protective function of UC-MSCs. Consistent with our hypothesis, dual-luciferase reporter experiments confirmed that miR-218-5p directly targets the CBX3 gene. CBX3, a key component of the HP1 family, is a known player in chromatin remodeling and transcriptional regulation. Our results suggest that CBX3 may serve as a potential bridge between epigenetic modification and ferroptosis in osteoblasts, although the precise downstream targets through which it modulates ferroptotic sensitivity require further elucidation.

Through functional gain and loss experiments, we have obtained evidence supporting a crucial role of CBX3 in this pathway: under the presence of UC-MSCs, overexpression of CBX3 significantly weakened its inhibitory effect on ferroptosis and its protective effect on osteogenic differentiation; while in the H_2O_2 treatment condition without UC-MSCs, knockdown of CBX3 could partially mimic the protective phenotype of UC-MSCs, restore the expression of anti-ferroptosis proteins and promote the levels of osteogenic markers(Bai et al. 2025). These bidirectional validation results suggest that UC-MSCs inhibit ferroptosis and promote osteogenic differentiation by up-regulating miR-218-5p and consequently down-regulating CBX3. However, the precise molecular mechanisms by which CBX3 regulates ferroptosis-related genes—including whether it directly or indirectly modulates the transcription of GPX4, SLC7A11, and FTH—require further investigation.

Several limitations of the current work must be acknowledged. Notably, the study relies exclusively on *in vitro* cell lines and lacks confirmation in living organisms. Because osteoporosis involves complex intercellular communication, future studies should assess the therapeutic relevance of this pathway in preclinical models, including OVX and aging-induced mouse models. Secondly, how UC-MSCs target and upregulate miR-218-5p in osteoblasts across the physical barrier in the indirect co-culture system remains a mystery. Considering the paracrine characteristics of mesenchymal stem cells, we strongly hypothesize that exosomes are the core delivery vehicles, which requires future confirmation through the extraction, identification, and purification of UC-MSC-Exos. Finally, it is plausible to hypothesize that CBX3 might directly or indirectly influence the transcription of ferroptosis defense genes such as GPX4. However, whether this regulation occurs via direct promoter binding or indirect signaling cascades remains speculative at this stage.

5 Conclusion

In summary, this study has revealed a novel epigenetic and metabolic regulatory pathway through which UC-MSCs alleviate the differentiation disorder of osteoblasts induced by oxidative stress. Our findings suggest that UC-MSCs can target and modulate the expression of CBX3 by upregulating miR-218-5p in damaged osteoblasts, thereby contributing to the maintenance of the GPX4/SLC7A11 defense system at both transcriptional and translational levels, strongly inhibiting the occurrence of lipid peroxidation and ferroptosis, and substantially restoring the differentiation and bone generation potential of osteoblasts.

This study not only provides new theoretical support for understanding the pathological mechanism of osteoporosis (especially the destructive role of ferroptosis in it), but also offers important molecular targets (miR-218-5p/CBX3 axis) for cell-free therapy based on UC-MSCs and their derivatives, demonstrating a broad clinical transformation prospect.

Abbreviations

Abbreviation	Full Form
ALP	Alkaline phosphatase
CBX3	Chromobox 3
CCK-8	Cell Counting Kit-8
cDNA	Complementary DNA
DCFH-DA	2',7'-Dichlorodihydrofluorescein diacetate
Fe^{2+}	Ferrous ion
FTH	Ferritin heavy chain
GPX4	Glutathione peroxidase 4
GSH	Glutathione
H_2O_2	Hydrogen peroxide
HRP	Horseradish peroxidase
LDH	Lactate dehydrogenase
MDA	Malondialdehyde
miRNA	MicroRNA
MSC	Mesenchymal stem cell
NC	Negative control
OCN	Osteocalcin
oe	Overexpression
PBS	Phosphate-buffered saline
PVDF	Polyvinylidene difluoride
ROS	Reactive oxygen species
RSL3	(1S,3R)-RSL3 (ferroptosis inducer)
RT-qPCR	Reverse transcription quantitative polymerase chain reaction
RUNX2	Runt-related transcription factor 2
SD	Standard deviation
SDS-PAGE	Sodium dodecyl sulfate–polyacrylamide gel electrophoresis
SEM	Standard error of the mean
si-CBX3	Small interfering RNA targeting CBX3

Abbreviation	Full Form
SLC7A11	Solute carrier family 7 member 11
UC-MSC	Umbilical cord mesenchymal stem cell
3'UTR	3'-Untranslated region

Declarations

Ethics approval and consent to participate

Not applicable.

Clinical trial number

Not applicable.

Consent for publication

All authors have read and approved the final manuscript and consent to its publication.

Availability of data and materials

The datasets used and/or analysed during the current study are available from the corresponding author on reasonable request.

Competing Interests

The authors declare that they have no competing financial interests or personal relationships that could have appeared to influence the research presented in this paper.

Funding

This research was funded by the Basic Research Program of the Yunnan Provincial Science and Technology Department (Project Number: 202401BA070001-077) and the Special Basic Research Program of the Yunnan Provincial Science and Technology Department (Project Number: 202601AT070055; Project Name: The mechanism by which CBD promotes mitochondrial transfer and alleviates SIH through CD38).

Authors' contributions

L.L., Y.H. and Y.M. were responsible for data collection, *in vitro* experiments, as well as bioinformatics and statistical analysis. L.L. and Y.H. drafted the initial version. J.L. participated in data validation and method optimization. Y.C. conceived and directed the entire project, provided financial support, and revised the manuscript. Y.M. participated in the formulation of the experimental design and made

important suggestions for mechanism research. All authors participated in the interpretation of the results, reviewed and approved the final manuscript.

Acknowledgements

Not applicable.

References

1. Hernlund E, Svedbom A, Ivergård M, Compston J, Cooper C, Stenmark J, McCloskey EV, Jönsson B, et al. Osteoporosis in the European Union: medical management, epidemiology and economic burden. A report prepared in collaboration with the International Osteoporosis Foundation (IOF) and the European Federation of Pharmaceutical Industry Associations (EFPIA). Arch Osteoporos. 2013;8:136.
2. Salari N, Ghasemi H, Mohammadi L, Behzadi MH, Rabieenia E, Shohaimi SMohammadi. M 2021 The global prevalence of osteoporosis in the world: a comprehensive systematic review and meta-analysis. J Orthop Surg Res 16 609.
3. Manolagas SC. Birth and death of bone cells: basic regulatory mechanisms and implications for the pathogenesis and treatment of osteoporosis. Endocr Rev. 2000;21:115–37.
4. Ye Y, Zhong H, Huang S, Lai W, Huang Y, Sun C, Zhang YZheng. S 2023 Reactive Oxygen Species Scavenging Hydrogel Regulates Stem Cell Behavior and Promotes Bone Healing in Osteoporosis. Tissue Eng Regen Med 20 981–92.
5. Shen X, Fang K, Ru Yie KH, Zhou Z, Shen Y, Wu S, Zhu Y, Deng Z et al. 2022 High proportion strontium-doped micro-arc oxidation coatings enhance early osseointegration of titanium in osteoporosis by anti-oxidative stress pathway. Bioact Mater 10 405–19.
6. Li C, Liu Y, Deng M, Li J, Li S, Li X, Zuo Y, Shen C et al. 2024 Comparison of the therapeutic effects of mesenchymal stem cells derived from human dental pulp (DP), adipose tissue (AD), placental amniotic membrane (PM), and umbilical cord (UC) on postmenopausal osteoporosis. Front Pharmacol 15 1349199.
7. Liu C, Zhang H, Tang X, Feng R, Yao G, Chen W, Li W, Liang J et al. 2018 Mesenchymal Stem Cells Promote the Osteogenesis in Collagen-Induced Arthritic Mice through the Inhibition of TNF-α. Stem Cells Int 2018 4069032.
8. Ru Q, Li Y, Chen L, Wu Y, Min JWang. F 2024 Iron homeostasis and ferroptosis in human diseases: mechanisms and therapeutic prospects. Signal Transduct Target Ther 9 271.
9. Dixon S, JOlzmann JA. The cell biology of ferroptosis. Nat Rev Mol Cell Biol. 2024;25:424–42.
10. Ruan B, Dong J, Wei F, Huang Z, Yang B, Zhang L, Li C, Dong H et al. 2024 DNMT aberration-incurred GPX4 suppression prompts osteoblast ferroptosis and osteoporosis. Bone Res 12 68.
11. Wang J, Chen TGao. F 2024 Mechanism and application prospect of ferroptosis inhibitors in improving osteoporosis. Front Endocrinol (Lausanne). 151492610.

12. Rahyussalim AJ, Al As'ady FM, Nasser M, KKurniawati T. Comprehensive approach to degenerative spine with fragility spine fracture to improve quality of life: A case report study. Int J Surg Case Rep. 2023;105:107978.
13. Iantomasi T, Romagnoli C, Palmini G, Donati S, Falsetti I, Miglietta F, Aurilia C, Marini F et al. 2023 Oxidative Stress and Inflammation in Osteoporosis: Molecular Mechanisms Involved and the Relationship with microRNAs. Int J Mol Sci 24.
14. Philippe S, Delay M, Macian N, Morel VPickering ME. 2023 Common miRNAs of Osteoporosis and Fibromyalgia: A Review. Int J Mol Sci 24.
15. Zhou Q, Zhou LLi J. MiR-218-5p-dependent SOCS3 downregulation increases osteoblast differentiation inpostmenopausal osteoporosis. J Orthop Surg Res. 2023;18:109.
16. Wu C, Liu X, Zhao B, Zhao M, Zhang B, Huang G, Cheng Y, Zheng S et al. 2026 CBX3 confers ferroptosis resistance during blood-borne metastasis. J Hematol Oncol 19 9.
17. Subarajan P, Arceo-Mendoza R, MCamacho PM. Postmenopausal Osteoporosis: A Review of Latest Guidelines. Endocrinol Metab Clin North Am. 2024;53:497–512.
18. Fischer VHaffner-Luntzer M. Interaction between bone and immune cells: Implications for postmenopausal osteoporosis. Semin Cell Dev Biol. 2022;123:14–21.
19. Yao Y, Cai X, Chen Y, Zhang MZheng. C 2025 Estrogen deficiency-mediated osteoimmunity in postmenopausal osteoporosis. Med Res Rev 45 561–75.
20. Hoang DM, Pham PT, Bach TQ, Ngo ATL, Nguyen QT, Phan TTK, Nguyen GH, Le PTT et al. 2022 Stem cell-based therapy for human diseases. Signal Transduct Target Ther 7 272.
21. Zhidu S, Ying T, Rui JChao. Z 2024 Translational potential of mesenchymal stem cells in regenerative therapies for human diseases: challenges and opportunities. Stem Cell Res Ther 15 266.
22. Dixon S, JStockwell B. R 2014 The role of iron and reactive oxygen species in cell death. *Nat Chem Biol.* 10 9–17.
23. Battaglia AM, Chirillo R, Aversa I, Sacco A, Costanzo FBiamonte. F 2020 Ferroptosis and Cancer: Mitochondria Meet the Iron Maiden Cell Death. Cells 9.
24. Xia Y, Ge G, Xiao H, Wu M, Wang T, Gu C, Yang HGeng. D 2023 REPIN1 regulates iron metabolism and osteoblast apoptosis in osteoporosis. Cell Death Dis 14 631.
25. Svajger U, Zajc K, Cesnik ABHK. Pooled umbilical cord-derived MSCs retain key phenotypic and immunomodulatory properties - A path toward consistent manufacturing. Tissue Cell. 2025;96:103036.
26. Shen C, Yang C, Xu SZhao. H 2019 Comparison of osteogenic differentiation capacity in mesenchymal stem cells derived from human amniotic membrane (AM), umbilical cord (UC), chorionic membrane (CM), and decidua (DC). Cell Biosci 9 17.
27. Kim JW, Min DW, Kim D, Kim J, Kim MJ, Lim HLee. J Y 2023 GPX4 overexpressed non-small cell lung cancer cells are sensitive to RSL3-induced ferroptosis. *Sci Rep.* 13 8872.

28. Xiao J, Feng N, Li Q, Cao X, Huang Q, Zhou B, Fan Z, Wei L et al. 2025 Mitochondria-specific GPX4 inhibition enhances ferroptosis and antitumor immunity. J Control Release 383 113841.
29. Zhang L, Li Y, Dong YC, Guan CY, Tian S, Lv XD, Li JH, Su X et al. 2022 Transplantation of umbilical cord-derived mesenchymal stem cells promotes the recovery of thin endometrium in rats. Sci Rep. 12 412.
30. Xu XH, Yuan TJ, Dad HA, Shi MY, Huang YY, Jiang Z, HPeng LH. Plant Exosomes As Novel Nanoplatforms for MicroRNA Transfer Stimulate Neural Differentiation of Stem Cells In Vitro and In Vivo. Nano Lett. 2021;21:8151–9.
31. Saadh MJ, Ahmed HH, Sanghvi G, Bin Awang Isa MZ, Singh P, Kaur K, Kumar M. RHusseen B 2025 Recent advances in the delivery of microRNAs via exosomes derived from MSCs, and their role in regulation of ferroptosis. Pathol Res Pract 270 155984.
32. Bai X, Duan T, Shao J, Zhang Y, Xing G, Wang J, Liu X, Wang M, et al. CBX3 promotes multidrug resistance by suppressing ferroptosis in colorectal carcinoma via the CUL3/NRF2/GPX2 axis. Oncogene. 2025;44:1678–93.

Figures

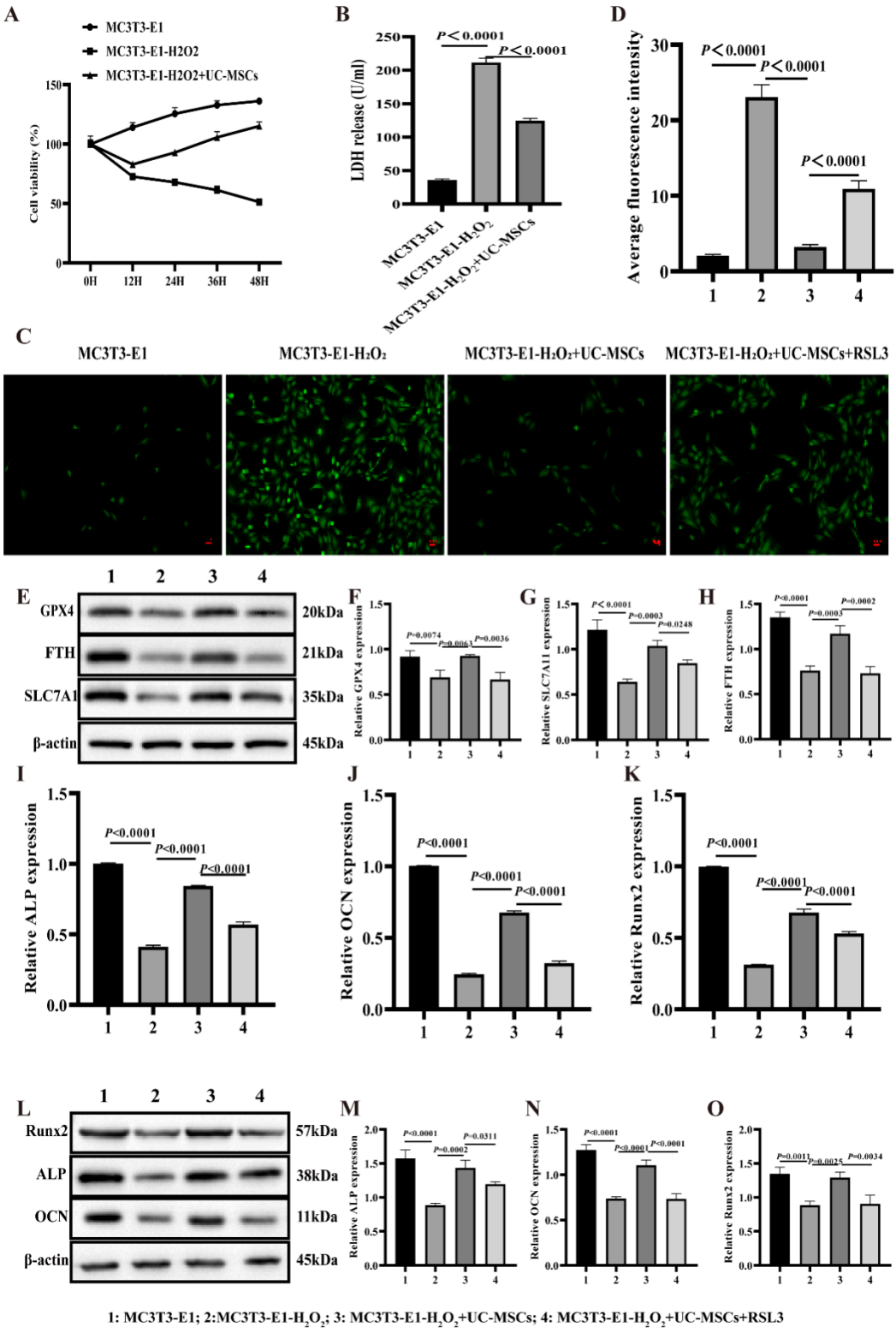


Figure 1

UC-MSCs protect osteoblasts from H_2O_2-induced damage and differentiation disorders by inhibiting the ferroptosis pathway. (A) At 0, 12, 24, 36, and 48 hours, the cell survival rate of different groups of MC3T3-E1 cells was detected using the CCK-8 method. (B) The release of LDH in the supernatant was measured. (C) Representative fluorescence images of intracellular ROS after DCFH-DA staining (scale = 50 μm). (D) Quantitative analysis of the average ROS fluorescence intensity. (E-H) Western blot analysis

and corresponding quantitative analysis of ferroptosis-related proteins GPX4, FTH, and SLC7A11. (I-K) RT-qPCR analysis of the relative mRNA expression levels of osteogenic markers ALP, OCN, and Runx2. (L-O) Western blot analysis and corresponding quantitative analysis of osteogenic proteins Runx2, ALP, and OCN. β-actin was used as a loading control. Groups: 1: MC3T3-E1; 2:MC3T3-E1-H_2O_2; 3: MC3T3-E1-H_2O_2+UC-MSCs; 4: MC3T3-E1-H_2O_2+UC-MSCs+RSL3. The data are presented as mean ± SD, and all are derived from n = 3 independent biological replicates. The exact *P* value is indicated above the bars; *P* < 0.0001 indicates the highest statistical significance level.

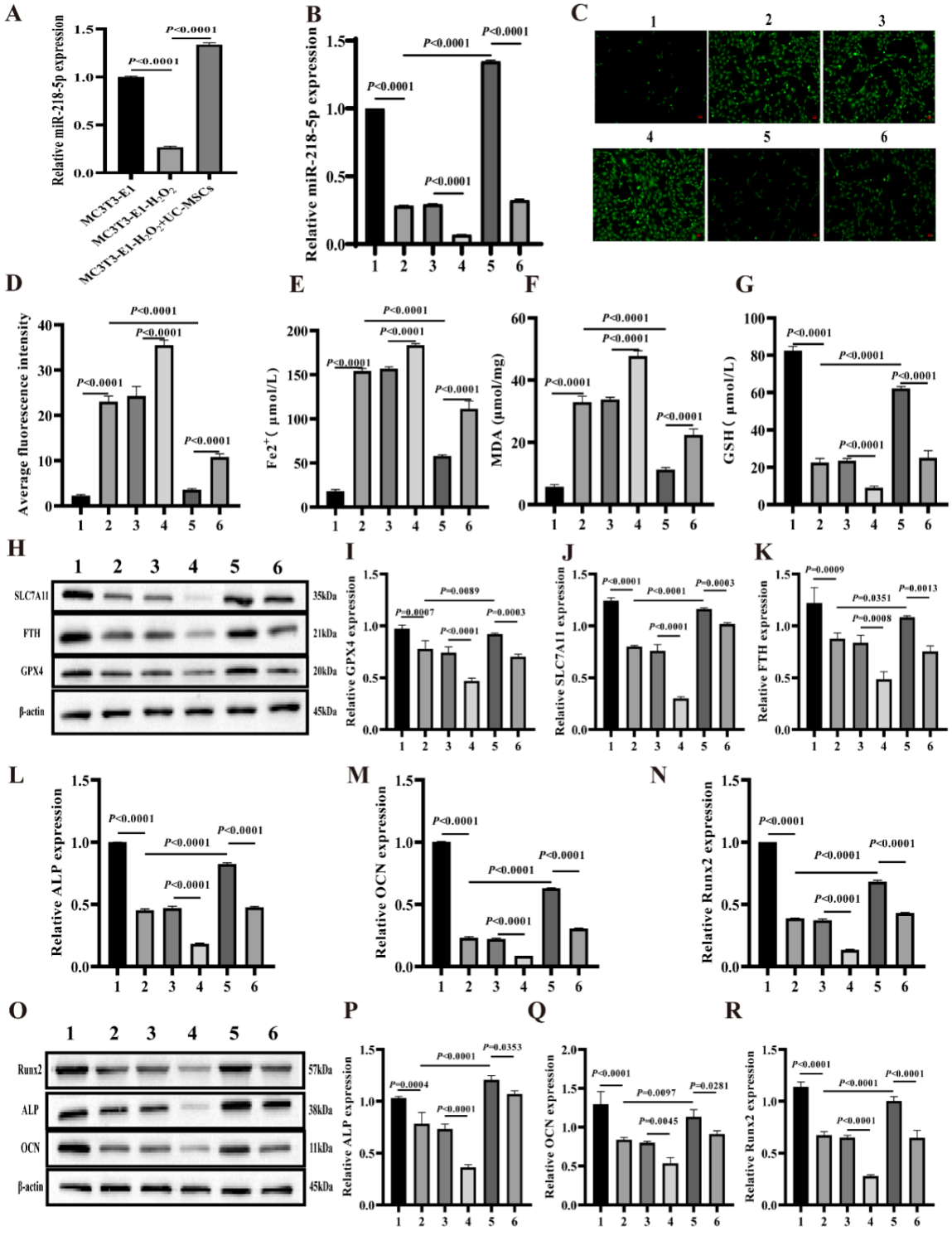


Figure 2

Inhibition of miR-218-5p can weaken the protective effect of UC-MSCs against H_2O_2-induced ferroptosis and osteogenic damage. (A-B) RT-qPCR was used to detect the expression levels of miR-218-5p in each group. (C-D) DCFH-DA staining was used to observe the accumulation of intracellular ROS (scale = 50 μm) and to quantify the fluorescence intensity. (E-G) The contents of Fe^{2+}, MDA, and GSH in each group of cells were detected. (H-K) Western blot was used to detect the expression and gray-scale

quantification of iron death defense proteins GPX4, SLC7A11, and FTH. (L-M) RT-qPCR was used to detect the relative mRNA expression levels of osteogenic-related genes ALP, OCN, and Runx2. β-actin was used as the internal reference for mRNA and protein detection, and U6 was used as the internal reference for miRNA detection. (O-R) Western blot was used to detect the expression and gray-scale quantification of osteogenic marker proteins Runx2, ALP, and OCN. Note: 1: MC3T3-E1; 2: MC3T3-E1-H_2O_2; 3: MC3T3-E1-NC-inhibitor- H_2O_2; 4: MC3T3-E1-miR-218-5p-inhibitor-H_2O_2; 5: MC3T3-E1-H_2O_2+UC-MSCs; 6: MC3T3-E1-miR-218-5p-inhibitor-H_2O_2+UC-MSCs. The data are presented as mean ± SD, and all are derived from n = 3 independent biological replicates. The exact *P* values or significance levels are indicated in the figure (**** *P* < 0.0001).

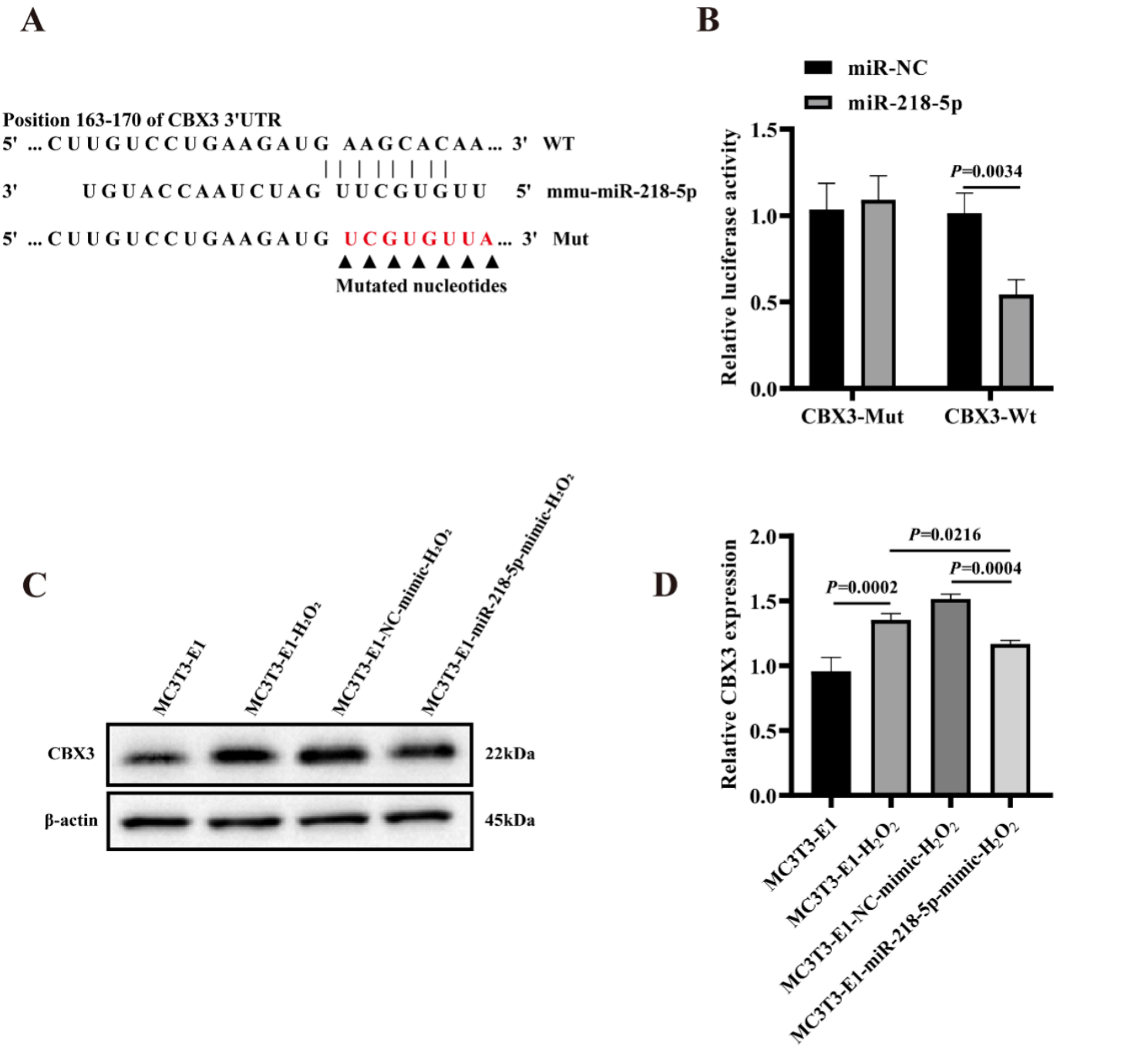


Figure 3

miR-218-5p targets and negatively regulates the expression of CBX3. (A) Bioinformatics predicts the binding sites of miR-218-5p to the 3'UTR region of mouse CBX3, and displays the mutant (Mut) sequence. (B) Dual luciferase reporter gene assay verifies the targeting relationship between miR-218-5p and the CBX3 3'UTR. (C-D) Western blot and gray-scale quantitative analysis detect the expression levels of CBX3 protein in different treatment groups. β-actin is used as the internal reference for protein detection. The data are presented as mean ± SD, and all come from n = 3 independent biological replicates. The exact *P* values have been marked in the figure to indicate statistical significance.

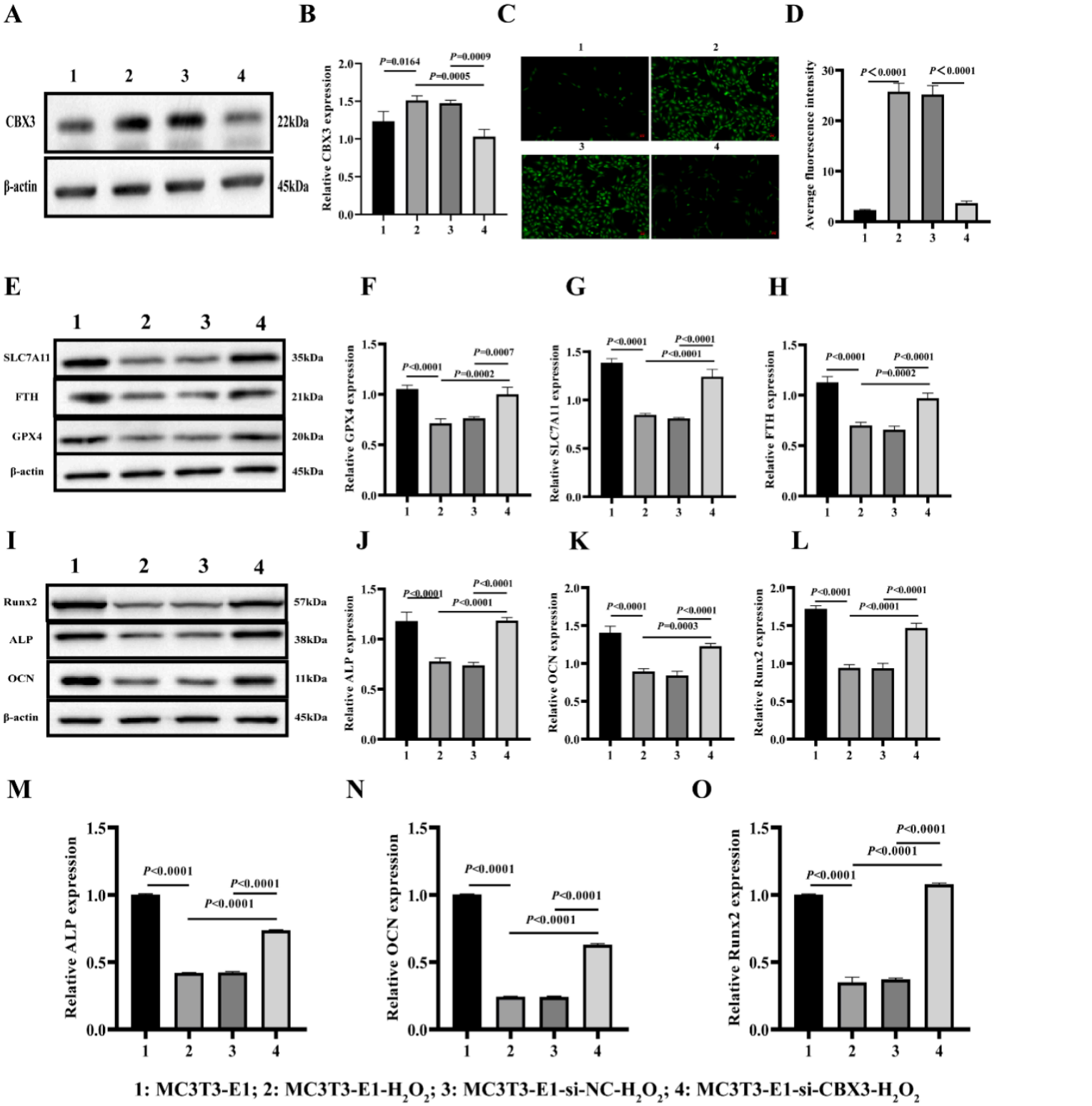


Figure 4

Targeted silencing of CBX3 can alleviate H_2O_2-induced osteoblast ferroptosis and osteogenesis disorder. (A-B) Western blot and gray-scale quantitative analysis verified the expression levels of CBX3 in different treatment groups and the knockdown efficiency of si-CBX3. (C-D) DCFH-DA fluorescence staining observed the accumulation of ROS in cells of each group (scale = 50 μm) and the average fluorescence intensity quantification. (E-H) Western blot and gray-scale quantitative analysis detected the protein

expression of ferroptosis defense proteins GPX4, SLC7A11, and FTH. (I-L) Western blot detected the expression levels of osteogenic marker proteins Runx2, ALP, and OCN and their corresponding gray-scale quantification. (M-O) RT-qPCR detected the relative mRNA expression levels of osteogenic marker genes ALP, OCN, and Runx2. β-actin was used as the internal reference for protein and mRNA detection. Group description: 1: MC3T3-E1; 2: MC3T3-E1-H_2O_2; 3: MC3T3-E1-si-NC-H_2O_2; 4: MC3T3-E1-si-CBX3-H_2O_2. The data are presented as mean ± SD, all derived from n = 3 independent biological replicates. The exact P values for the key comparison groups are shown in the figure; $P < 0.0001$ indicates a statistically significant difference of extreme magnitude.

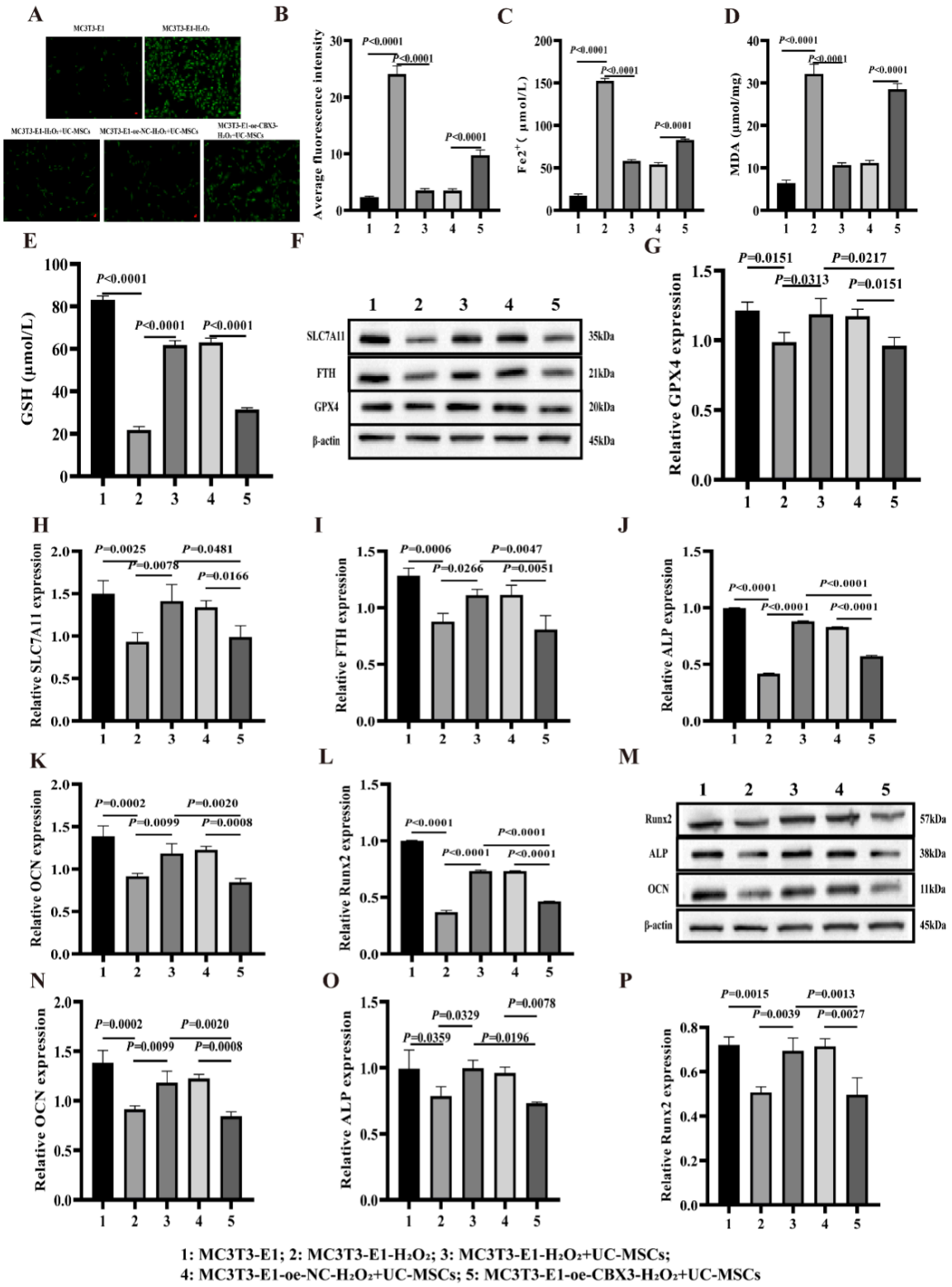


Figure 5

Overexpression of CBX3 reversed the protective effect of UC-MSCs on H_2O_2-induced ferroptosis and osteogenic dysfunction. (A-B) DCFH-DA fluorescence staining was used to observe the accumulation of ROS in cells of each group (scale = 50 μm) and to quantify the average fluorescence intensity. (C-E) Biochemical assays were used to detect the changes in Fe^{2+}, MDA, and GSH contents in cells of each group. (F-I) Western blot and gray-scale quantitative analysis were used to detect the expression levels

of ferroptosis defense proteins GPX4, SLC7A11, and FTH. (J-L) RT-qPCR was used to detect the relative mRNA expression levels of osteogenic marker genes ALP, OCN, and Runx2 in each group. (M-P) Western blot and gray-scale quantitative analysis were used to detect the expression levels of osteogenic marker proteins Runx2, ALP, and OCN. β-actin was used as the internal reference for protein and mRNA detection. Group description: 1: MC3T3-E1; 2: MC3T3-E1-H_2O_2; 3: MC3T3-E1-H_2O_2+UC-MSCs;4: MC3T3-E1-oe-NC-H_2O_2+UC-MSCs; 5: MC3T3-E1-oe-CBX3-H_2O_2+UC-MSCs. The data are presented as mean ± SD, all derived from n = 3 independent biological replicates. The exact *P* values for the key comparison groups are shown in the figure; $P < 0.0001$ indicates a statistically significant difference of extreme magnitude.

Supplementary Files

This is a list of supplementary files associated with this preprint. Click to download.

- Uncroppedgelsandblotsimages.pdf